[PROC. OF JSCE No. 352/III-2 (Geotechnical Eng.) December 1984]

LIQUEFACTION ANALYSIS OF SAND DEPOSITS BY AN ELASTIC-PLASTIC CONSTITUTIVE MODEL

By Hiroyoshi HIRAI and Masao SATAKE***

An elastic-plastic constitutive model is presented in this paper which is capable of describing the cyclic behavior of sands reasonably accurately. A non-associated flow rule is used by modifying the model available to monotonic loadings. Undrained cyclic triaxial tests are simulated and the results are compared with the experimental data. The numerical formulation and solution techniques are presented to analyze the dynamic behavior of sand deposits subjected to earthquake shocks. The characteristics related to liquefaction are investigated about the effective stress path, liquefaction zone and pore pressure. It was shown that the permeability coefficient can significantly influence the response of the ground during earthquakes.

1. INTRODUCTION

In the present decade remarkable advances have been made in the analysis for problems of grounds subjected to dynamic loadings. The dynamic behavior of a ground is generally dependent not only on the input motion but also on the constitutive relation of constituent soils. The nonlinear relationship appears in the hysteresis of stress and strain for soils. This nonlinearity has the great influence on the dynamic response of grounds. In order to incorporate the nonlinear hysteretic properties of soils into one-dimensional problems during dynamic cyclic loadings, the skeleton curves such as the bilinear model, Ramberg-Osgood[1] model and Hardin-Drnevich[2] model have been proposed. Recently, the general constitutive laws have been developed to describe more precisely the behavior of soils under cyclic stresses. The development of the constitutive models for dynamic response analysis is summarized in detail in the book edited by Pande et al.[3].

Although much research has been made for the description of deformation of soils under static conditions of stress, a universal, quantitative model generally acceptable has not yet been appeared. The situation becomes more complicated when fluctuating loads such as earthquake shock and traffic vibration occur. The constitutive model under cyclic loadings in drained states must accurately represent the following characteristics of the soil behavior :

(1) nonlinear hysteretic shear stress-strain relationship;

(2) accumulated irreversible volumetric strain.

Of the two features, the second is responsible for the increase of pore pressure during cyclic load applied to a sample where saturated and undrained behavior predominates. When the pore pressure builds up to a

* Member of JSCE Dr. Eng., Research Associate. Department of Civil Engineering, Tohoku University.
** Member of JSCE Dr. Eng., Professor, Department of Civil Engineering, Tohoku University. (Aoba, Sendai, 980)

value of mean total compressive stress, the effective stress state reaches the failure of the material. This is referred to as liquefaction generally.

An elastic-plastic constitutive model based on the non-associated flow rule has been proposed by Hirai et al.[4] for the description of sand behavior under static, monotonic loadings. This model can provide reasonable, accurate prediction if the range of usage for the model is restricted to the stress paths such as encountered in monotonic loadings. In the presentpaper, to reproduce the essential features of cyclic response, the constitutive model available to monotonic loads is modified or extended. This model is capable of quantitative predictions concerning the pore pressure increase evaluation. The numerical formulation and solution techniques for dynamic soil problems are presented. The discussion is made about the computed results for liquefaction characteristics of a ground during an earthquake.

2. STRESS-STRAIN RELATIONSHIPS OF SAND

Let $\dot{T}_{ij}$ and $\dot{E}_{ij}^{(p)}$ be stress rates and plastic strain rates respectively. On the basis of the principal of maximum plastic work called Drucker's postulate[5] and written as $\dot{T}_{ij}\dot{E}_{ij}^{(p)}\geqq 0$, Prager[6] formulated an associated flow rule. Let $f=0$ beyield function having a closed surface in the stress space. According to the relation established by Prager, no change in plastic deformation occurs as long as the stress exists inside of the yield function, i. e., $f<0$; however, the purely elastic behavior is not observed in the range $f<0$ during unloadings for geological materials such as clay, sand and rock. This may recall the noticeable remark, as pointed out by Prevost et al.[7], that Drucker's postulate is not the necessary condition but the sufficient condition for stability and uniqueness. Hill[8] derived a constitutive relation based on the non-associated flow rule, not introducing Drucker's postulate. Developing the formulation given by Hill, Prevost et al. discussed the strain softening flow rule violating Drucker's postulate. The stress-strain relationship during repeated loadings will be investigated by elaborating the formulation shown by Hill in what follows. Requiring that the principal axes of the plastic strain increment tensor must coincide with the principal stress axes since the element is isotropic, we can satisfy this condition by assuming that

$$\dot{E}_{ij}^{(p)}=\Lambda\frac{\partial g}{\partial T_{ij}} \quad (1)$$

where g is called a plastic potential, Λ is a scalar function and g and Λ may be represented in terms of invariants of stress and plastic strain. Assuming the work-hardening parameter γ to be a function of the plastic strain, we can express the consistency condition given by Prager[6] in the form

$$\dot{f}=\frac{\partial f}{\partial T_{ij}}\dot{T}_{ij}+\frac{\partial f}{\partial E_{ij}^{(p)}}\dot{E}_{ij}^{(p)}+\frac{\partial f}{\partial \gamma}\frac{\partial \gamma}{\partial E_{ij}^{(p)}}\dot{E}_{ij}^{(p)}=0 \quad (2)$$

This means that loading from a plastic state must lead to another plastic state. Substituting Eq. (1) into Eq. (2) and solving for Λ, we obtain

$$\dot{E}_{ij}^{(p)}=h\frac{\partial g}{\partial T_{ij}}\frac{\partial f}{\partial T_{kl}}\dot{T}_{kl} \quad (3)$$

where

$$h=-1/\left\{\left(\frac{\partial f}{\partial E_{mn}^{(p)}}+\frac{\partial f}{\partial \gamma}\frac{\partial \gamma}{\partial E_{mn}^{(p)}}\right)\frac{\partial g}{\partial T_{mn}}\right\} \quad (4)$$

It should be noticed that above derivation does not count on Drucker's postulate being essential basis of the associated flow rule proposed by Prager. The formulation similar to Eq. (3) is found in the constitutive relation shown by Nova[9]. The non-associated flow rule generally violates Drucker's postulate, since the relation that $\dot{T}_{ij}\dot{E}_{ij}^{(p)}\geqq 0$ does not necessarily hold due to the difference between yield function and plastic potential. The salient feature of Eq. (3) is that it is applicable to the case where plastic deformation may occur for stress states within the yield surface. This feature yields definite advantages over the conventional non-associated flow rules. From the viewpoint above, the yield function in the present paper only designates the difference between two states on and inside the yield surface.

In order to describe the inelastic behavior within the yield surface, the new concept referred to as the boundary or bounding surface is proposed by Mroz et al.[10] and Dafalias et al.[11]. The stress-strain relations can predict to some extent the plastic behavior during cyclic loadings. To describe the behavior during repeated loading of normally and overconsolidated saturated sands, Nishi[12] performed undrained cyclic tests and proposed an elastic-plastic constitutive model. For cyclic behavior of sands, Ghaboussi et al.[13] showed a material model where a non-associated flow rule is used and the volumetric strain is determined by a semi-empirical rule.

For sand, Hirai et al.[4] discussed the capability of several models related to the associated and non-associated flow rules. Among them, the model based on the non-associated flow rule possesses simple, reasonable forms of yield functions and plastic potentials

$$f_1=J_2+\beta I_1^2+\gamma_1 I_1=0 \quad (5)$$

$$f_2=I_1+\gamma_2=0 \quad (6)$$

and

$$g_1=J_2^{1/2}/I_1-M\ln|I_1/I_0|=0 \quad (7)$$

$$g_2=I_1+\gamma_2=0 \quad (8)$$

where f_1 and g_1 are called the modified Cam clay and Cam clay models respectively, the combination of f_2 and g_2 is related to consolidation, $J_2=T'_{ij}T'_{ij}/2$ is the second invariant of the deviatoric stress T'_{ij}, $I_1=T_{kk}$ is the first invariant of stress, β and$M$ are material constants and γ_1, γ_2 and I_0 denote work-hardening parameters. The rates of the work-hardening parameters γ_1 and γ_2 are given by

$$\dot{\gamma}_1=\phi_1 T_{ii}\dot{E}_{jj}^{(p)}/3+\phi_2 T'_{ij}\dot{E}_{ij}^{(p)} \quad (9)$$

$$\dot{\gamma}_2=\psi_1 T_{ii}\dot{E}_{jj}^{(p)}/3 \quad (10)$$

where ϕ_1, ϕ_2 and ψ_1 are material constants.

The undrained triaxial compression tests of sand performed by Ishihara et al.[14] suggest that, for one cycle of unloading and subsequent reloading,

a) The deviatoric plastic strain may be assumed not to occur since the reloading process traces the same path as that along which the unloading has been excuted, in the relation between the deviatoric strain and the axial difference stress.

b) It may be assumed that no volumetric plastic strain generates if the stress stays below the phase transformation line defined as $-J_2^{1/2}/I_1=M$.

c) The volumetric plastic strain conspicuously appears once the stress state has been kept beyond the phase transformation line.

When no plastic strain due to consolidation occurs, i.e., Eqs. (6), (8) and (10) are neglected, the suggestion mentioned above indicates that

1) If $f=0$ and $\partial f_1/\partial T_{ij}\dot{T}_{ij}\geqq 0$, the forms of Eqs. (5), (7) and (9) are employed.

2) If $f_1<0$ or $\partial f_1/\partial T_{ij}\dot{T}_{ij}<0$ and $(-J_2^{1/2}/I_1)_{\max}\leq M$, the behavior of sand is assumed to be elastic.

3) If $f_1<0$ or $\partial f_1/\partial T_{ij}\dot{T}_{ij}<0$ and $(-J_2^{1/2}/I_1)_{\max}>M$, the other forms are adopted as

$$f_3=J_2+\beta I_1^2+\gamma_3 I_1=0 \quad (11)$$

$$g_3=I_1+\gamma_4=0 \quad (12)$$

$$\dot{\gamma}_3=\phi_2 T_{ii}\dot{E}_{jj}^{(p)}/3 \quad (13)$$

where f_3 and g_3 are yield function and plastic potential respectively, γ_3 and γ_4 are work-hardening parameters and ϕ_2 is a material constant. In case (3), the domain enclosed by the yield surface f_1 is not elastic and, for stress trajectories within this surface, plastic flow occurs as the yield function f_3 contracts or expands, according as unloading or reloading.

The constitutive equation in the elastic state is expressed as

$$T_{ij}=C_{ijkl}E_{kl}^{(e)} \quad (14)$$

where C_{ijkl} are components of the tensor of elastic constant and $E_{ij}^{(e)}$ are components of elastic strain. Since the strain rate is decomposed into elastic and plastic parts

$$\dot{E}_{ij}=\dot{E}_{ij}^{(e)}+\dot{E}_{ij}^{(p)} \quad (15)$$

we get the total stress-strain incremental ralation in the form

$$\dot{T}_{ij}=D_{ijkl}\dot{E}_{kl} \quad (16)$$

where

$$D_{ijkl}=C_{ijkl}-M_{ijkl} \quad (17)$$

$$M_{ijkl}=C_{ijpq}\frac{\partial g}{\partial T_{pq}}\frac{\partial f}{\partial T_{mn}}C_{mnkl}\Big/\left(-\frac{\partial f}{\partial \gamma}\frac{\partial \gamma}{\partial E_{st}^{(p)}}\frac{\partial g}{\partial T_{st}}+C_{stuv}\frac{\partial f}{\partial T_{st}}\frac{\partial g}{\partial T_{uv}}\right) \quad (18)$$

As the shear stress increases, failure occurs with the infinity of strains. The failure criterion proposed by Drucker and prager[15] is expressed as

$$F=J_2^{1/2}+\xi I_1=0 \quad (19)$$

where ξ is a material constant. There are many uncertainties in the behavior of soils after failure. For convenience, it is assumed that the stress-strain relation after failure requires the elastic model

$$T_{ij}=\bar{C}_{ijkl}E_{kl} \quad (20)$$

where $\bar{C}_{ijkl}$ are elastic constants in loading after failure and are assumed to be $\bar{C}_{ijkl}=C_{ijkl}/100$.

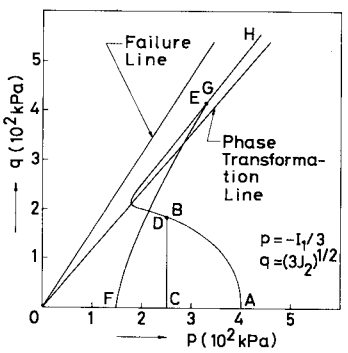

Fig. 1 Effective stress path computed under undrained cyclic condition.

By use of the combination of Eqs. (5), (7) and (9) and the other one of Eqs. (11) to (13), the effective stress path designated by the curve A to H for undrained triaxial compression test with repeated loading is calculated, as shown in Fig. 1. The notations $p=-I_1/3$ and $q=(3J_2)^{1/2}$ are employed in Fig. 1. The part of the curve, $ABGH$, corresponds to the effective stress path during the monotonic loading. Since the elastic behavior assumed in the part BCD, no increment of pore pressure takes place. The effective stress p decreases as the axial difference stress q decreases from $EtoF$, while, the effective stress p increases with the increase of q from F to G. The trend similar to the results shown above is observed in the experimental data given by Ishihara et al.[14].

3. ANALYTICAL FORMULATION OF GROUND MOTION

Consider the dynamic analysis of the ground subjected to earthquake shocks. The deviatoric stresses

$$s_{ij}=\sigma'_{ij}-\sigma'_{kk}\delta_{ij}/3 \quad (21)$$

are employed, where $\sigma'_{ij}=-T_{ij}$. The notation $\varepsilon_{ij}=-E_{ij}$ will be adopted later. Fig. 2 shows the horizontal surface layer on a base layer and the rectangular cartesian coordinates.

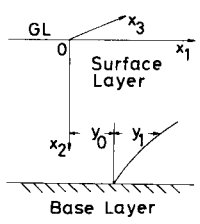

Fig. 2 A ground and coordinate system.

Since the ground is laid down under conditions of zero lateral strains, $\varepsilon_{11}=\varepsilon_{33}=0$, it is seen from Eq. (16) that the stress-strain relationship in the present problem is expressed as

$$\begin{Bmatrix}\dot{\sigma}'_{11}\\ \dot{\sigma}'_{22}\\ \dot{\sigma}'_{33}\\ \dot{\sigma}_{12}\end{Bmatrix}=\begin{bmatrix}D_{11} & D_{12}\\ D_{21} & D_{22}\\ D_{31} & D_{32}\\ D_{41} & D_{42}\end{bmatrix}\begin{Bmatrix}\dot{\varepsilon}_{22}\\ \dot{\varepsilon}_{12}\end{Bmatrix} \quad (22)$$

where for loading such that $f_1=0$ and $\partial f_1/\partial\sigma'_{ij}\dot{\sigma}'_{ij}\geqq 0$, it follows that

$$D_{11}=-I_1/(3\lambda)-2G/3-\{(J_2^{1/2}/I_1+M)/\lambda-Gs_{11}/(I_1J_2^{1/2})\}\times\{(J_2-\beta I_1^2)/\lambda-2Gs_{22}\}/B$$

$$D_{12}=\{(J_2^{1/2}/I_1+M)/\lambda-Gs_{11}/(I_1J_2^{1/2})\}4Gs_{12}/B$$

$$D_{21}=-I_1/(3\lambda)+4G/3-\{(J_2^{1/2}/I_1+M)/\lambda-Gs_{22}/(I_1J_2^{1/2})\}\times\{(J_2-\beta I_1^2)/\lambda-2Gs_{22}\}/B$$

$$D_{22}=\{(J_2^{1/2}/I_1+M)/\lambda-Gs_{22}/(I_1J_2^{1/2})\}4Gs_{12}/B$$

$$D_{31}=D_{11},\quad D_{32}=D_{12}$$
$$D_{41}=Gs_{12}\{(J_2-\beta I_1^2)/\lambda-2Gs_{22}\}/(I_1J_2^{1/2}B)$$
$$D_{42}=2G-4G^2s_{12}^2/(I_1J_2^{1/2}B)$$
$$B=(\phi_1-\phi_2)J_2^{1/2}+M\phi_1I_1+\{2GJ_2^{1/2}-(J_2-\beta I_1^2)\times(M+J_2^{1/2}/I_1)3/\lambda\}/I_1 \quad (23)$$

and for the stress state like that $f_1<0$ or $\partial f_1/\partial\sigma'_{ij}\dot{\sigma}'_{ij}<0$ and $(-J_2^{1/2}/I_1)_{\max}>M$, we obtain

$$D_{11}=-I_1/(3\lambda)-2G/3-I_1\{(J_2-\beta I_1^2)/\lambda-2Gs_{22}\}/(\lambda B)$$
$$D_{12}=4Gs_{12}I_1/(\lambda B)$$
$$D_{21}=-I_1/(3\lambda)+4G/3-I_1\{(J_2-\beta I_1^2)/\lambda-2Gs_{22}\}/(\lambda B)$$
$$D_{22}=4Gs_{12}I_1/(\lambda B),\quad D_{31}=D_{11},\quad D_{32}=D_{12},\quad D_{41}=0$$
$$D_{42}=2G,\quad B=(\phi_2+3\beta/\lambda)I_1^2-3J_2/\lambda \quad (24)$$

In the above, λ is a material constant defined as $\dot{\varepsilon}_{kk}^{(e)}=\lambda\dot{\sigma}'_{jj}/\sigma'_{ii}$ and G is the elastic shear modulus.

Since the total stress in the vertical direction σ_{22} is assumed to be constant, we have

$$\dot{\sigma}'_{22}=-\dot{u} \quad (25)$$

where u denotes the pore pressure. Using Eqs. (22) and (25) leads to

$$\dot{\sigma}_{12}=A_1\dot{\varepsilon}_{12}+A_2\dot{u} \quad (26)$$
$$\dot{\varepsilon}_{22}=C_1\dot{\varepsilon}_{12}+C_2\dot{u} \quad (27)$$

where

$$\left.\begin{aligned}A_1&=D_{42}-D_{22}D_{41}/D_{21}\\A_2&=-D_{41}/D_{21}\\C_1&=-D_{22}/D_{21}\\C_2&=-1/D_{21}\end{aligned}\right\} \quad (28)$$

The mixture theory for solid and fluid phases is first established by Biot[16], who extended it to the dynamic range limited to linear elastic behavior. Developing the Biot equations to deal with non-linear situations, Zienkiewicz et al.[17] showed an approximate but reasonable formulation of mixture theory in the form

$$\sigma_{ij,j}+\rho b_i=\rho\ddot{y}_i \quad (29)$$
$$u_{,i}+\rho_f b_i=\rho_f g/k\dot{w}_i+\rho_f\ddot{y}_i \quad (30)$$
$$\dot{\varepsilon}_{ii}=-\dot{w}_{i,i} \quad (31)$$

where $\sigma_{ij}=\sigma'_{ij}+u\delta_{ij}$, ρ is the density of solid plus fluid, b_i are body forces, y_i are relative displacements of solid matrix, k is the permeability coefficient, ρ_f denotes the density of the fluid alone, g is the gravitational acceleration, w_i represent the relative displacements of the fluid to the solid skeleton, ε_{ii} is the volumetric strain and $(\dot{\ })=\partial(\ )/\partial t$. The relation of Eq. (29) represents the overall equilibrium between the total stress-tensor gradients, body forces and inertia forces. In the dynamic case, the equilibrium of fluid flow is written as Eq. (30). Finally the mass balance of flow requires the relation of Eq. (31) when solid grains anq fluid are assumed to be imcompressible. Substituting Eq. (30) into Eq. (31) and assuming that $\ddot{w}_i=0$ leads to

$$u_{,ii}=-\rho_f g/k\dot{\varepsilon}_{ii} \quad (32)$$

This expresses an augmented form of the transient seepage equation.

The motion in the directions of x_1 and x_2 is considered in the surface layer on the base layer. Assuming that $\partial\sigma_{11}/\partial x_1=0$, we get from Eq. (29)

$$\partial\sigma_{12}/\partial x_2=\rho(\ddot{y}_1+\ddot{y}_0) \quad (33)$$

where $b_1=-y_0$ and y_0 is the displacement in x_1-direction of base layer. When it is assumed that $\partial u/\partial x_1=0$, Eq. (32) is expressed as

$$\frac{\partial^2 u}{\partial x_2^2}=-\frac{\rho_f g}{k}\frac{\partial}{\partial t}\varepsilon_{22} \quad (34)$$

Substitution of Eq. (26) into Eq. (33) leads to

$$\rho\frac{\partial^2\Delta y_1}{\partial t^2}-\frac{A_1}{2}\frac{\partial^2\Delta y_1}{\partial x_2^2}+\rho\frac{\partial^2\Delta y_0}{\partial t^2}-A_2\frac{\partial\Delta u}{\partial x_2}=0 \quad (35)$$

where Δy_1 is the displacement increment and

$$\varepsilon_{12}=\partial y_1/\partial x_2/2 \quad \cdots\cdots (36)$$

Substituting Eq. (27) into Eq. (34), we obtain

$$\frac{k}{\rho_f g}\frac{\partial^2 u}{\partial x_2^2}+C_2\frac{\partial u}{\partial t}+C_1\frac{\partial \varepsilon_{12}}{\partial t}=0 \quad \cdots\cdots (37)$$

Eqs. (35) and (37) form a coupled system of differential equations for fluid-solid dynamic interaction. The surface layer is divided in finite element mesh, as shown in Fig. 3. Applying the standard discretization procedure (e. g., Zienkiewicz[18]) to Eq. (35), we arrive simply at

$$[M]\{\Delta\ddot{Y}\}+[K]\{\Delta Y\}+\{\Delta F\}=0 \quad \cdots\cdots (38)$$

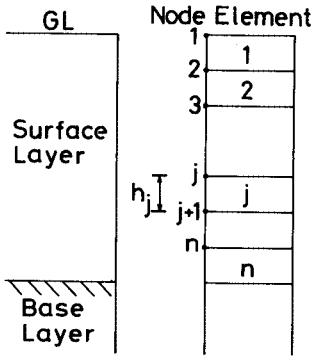

Fig. 3 Finite Element Division.

where matrices $[M]_j$ and $[K]_j$ of jth element and the force vector $\{\Delta F\}_j$ are given by

$$[M]_j=\rho_j h_j/6\begin{bmatrix}2 & 1\\ 1 & 2\end{bmatrix} \quad \cdots\cdots (39)$$

$$[K]_j=A_{1j}/(2h_j)\begin{bmatrix}1 & -1\\ -1 & 1\end{bmatrix} \quad \cdots\cdots (40)$$

$$\{\Delta F\}_j=\rho_j h_j/2\,\Delta\ddot{y}_0\begin{Bmatrix}1\\ 1\end{Bmatrix}+A_{2j}/2\begin{bmatrix}1 & -1\\ 1 & -1\end{bmatrix}\begin{Bmatrix}\Delta U_j\\ \Delta U_{j+1}\end{Bmatrix} \quad \cdots\cdots (41)$$

where ρ_j, h_j, A_{1j} and A_{2j} correspond to ρ, h, A_1 and A_2 of jth element respectively and

$$\{y_1\}=[N]\{Y\} \quad \cdots\cdots (42)$$

$$\{u\}=[N]\{U\} \quad \cdots\cdots (43)$$

In the above, $\{Y\}$ and $\{U\}$ represent displacements and pore pressures at nodes for a particular element respectively and $[N]$ is called the shape function

$$[N]=[h_j-x_2', x_2']/h_j \quad \cdots\cdots (44)$$

where x_2' is the local coordinate system.

The linear acceleration method formulated by Newmark[19] is used to solve Eq. (38). The flow equation (37) similarly yields a discrete form

$$[S]\{U\}+[T]\{\dot{U}\}+\{P\}=0 \quad \cdots\cdots (45)$$

where matrices $[S]_j$ and $[T]_j$ of jth element and the vector $\{P\}_j$ are expressed by

$$[S]_j=k_j/(\rho_f g h_j)\begin{bmatrix}1 & -1\\ -1 & 1\end{bmatrix} \quad \cdots\cdots (46)$$

$$[T]_j=-C_{2j}h_j/6\begin{bmatrix}2 & 1\\ 1 & 2\end{bmatrix} \quad \cdots\cdots (47)$$

$$\{P\}_j=-C_{1j}h_j(\dot{\varepsilon}_{12})_j/2\begin{Bmatrix}1\\ 1\end{Bmatrix} \quad \cdots\cdots (48)$$

where k, C_{1j}, C_{2j} and $(\varepsilon_{12})_j$ denote k, C_1, C_2 and ε_{12} of jth element respectively. The step-by-step process given by Zienkiewicz et al.[20] can be applied to Eq. (45).

4. NUMERICAL RESULTS AND DISCUSSIONS

A site in Niigata city where the earthquake occurred in 1964 is adopted as the ground model for computation. The total depth of the surface sand layer is 30 m and the water table is 2 m in depth. The distribution of the relative density of sand is the same as that used by Oka et al.[21], as shown in Fig. 4. Other parameters of sand deposits are determined as follows:

(1) The void ratio, e, is determined from the relative density D_r,

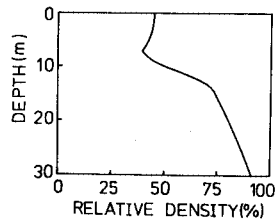

Fig. 4 The relative density of sand deposits used in computation.

the maximum void ratio e_{max} and the minimum void ratio e_{min} in the form

$$e=e_{max}-D_r(e_{max}-e_{min}) \quad (49)$$

(2) The mass density, ρ, of soil is obtained by use of

$$\rho=(G_s+e)/(1+e) \quad (50)$$

where G_s is the specific gravity of soil particles.

(3) The permeability coefficient k is simply defined by the relation given by Taylor :

$$k=Ce^3/(1+e) \quad (C : \text{constant}) \quad (51)$$

In the calculation, the permeability coefficient of the element at the ground surface is specified.

(4) The elastic shear modulus is determined with the aid of the method proposed by Seed et al.[22] (Eqs. (2) and (4) in 22)).

(5) The soil parameters M, β, ϕ_1, ϕ_2 etc. in the proposed constitutive relation are connected with the relative density of sands. For convenience, however, according to the experimental data given by Hirai et al.[4], it is assumed that

$$G_s=2.65,\ e_{max}=0.99,\ e_{min}=0.61,$$
$$\lambda=6.34\times10^{-4},\ M=0.228,\ \beta=1.33\times10^{-2}$$
$$\phi_1=86.9,\ \phi_2=21.7,\ \xi=0.289,\ \psi_2=-5.56\times10^2 \quad (52)$$

where the value of ψ_2 above is determined to satisfy the results shown in Fig. 1 and the following values are adopted :

$$h_j=1\,\text{m},\ \Delta t=0.001\,\text{sec},\ K_0=\sigma'_{11(0)}/\sigma'_{22(0)}=0.5 \quad (53)$$

where $\sigma'_{ij(0)}$ are initial effective stresses.

Fig. 5 shows the acceleration record observed at the gallery of Tarumizu dam when 1978 Miyagiken-oki earthquake occurred. This record is employed as the input base acceleration. Fig. 6 demonstrates the relationship between the shear stress σ_{12} and shear strain ε_{12} at the depth 9.5 m for the permeability coefficient $k=10^{-4}$ m/s and it is seen that the nonlinear hysteretic property appears as the shear stress is repeated. Fig. 7 depicts the relations between the shear strain and time and it is found that for $k=10^{-4}$ m/s the shear strain abruptly increases to reach liquefaction at 5.68 sec ; however, for $k=10^{-3}$ m/s liquefaction or failure does not occur. The computation for $k=10^{-4}$ m/s is not carried out after liquefaction, because the constitutive model presented here is not available to the description of the state

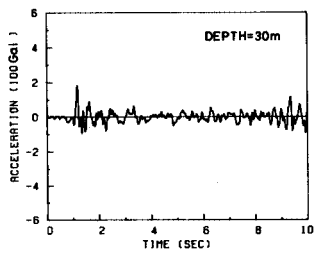

Fig. 5 Acceleration record.

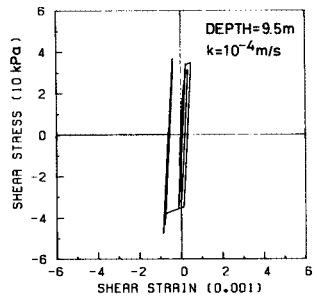

Fig. 6 Stress-strain relation.

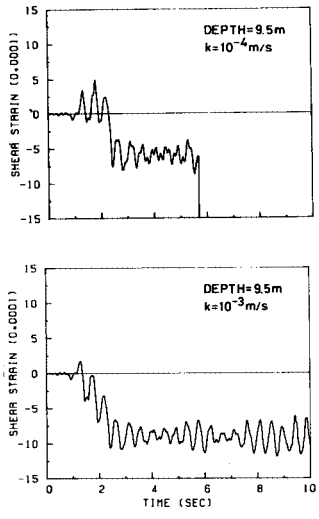

Fig. 7 Strain time history.

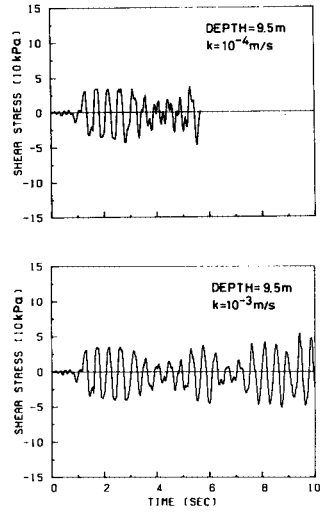

Fig. 8 Stress time history.

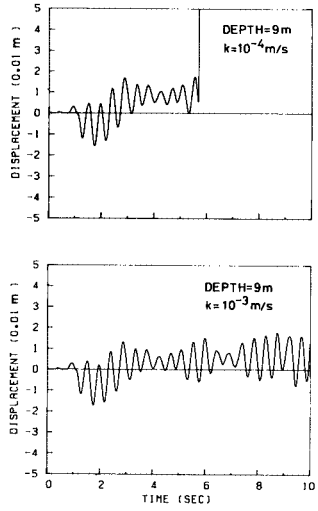

Fig. 9 Displacement time history.

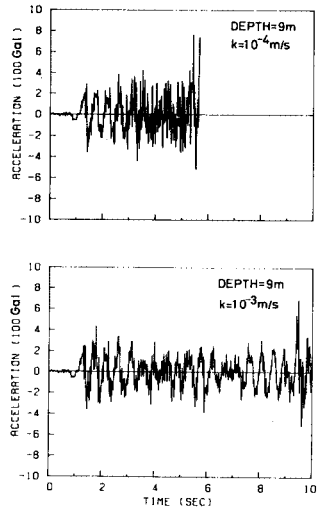

Fig. 10 Acceleration time history.

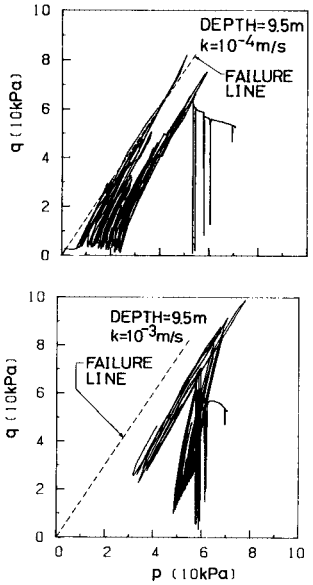

Fig. 11 Effective stresses p-q relation.

of the zero effective mean principal stress. Fig. 8 shows the relations between the shear stress and time and it is noticed that the shear stress is hardly affected by the magnitude of the permeability coefficient.

Fig. 9 exhibits the relations between displacement and time at 9 m in depth. The sudden increase of the displacement for $k=10^{-4}$ m/s accounts for the occurrence of liquefaction. Fig. 10 demonstrates the relation between acceleration and time at 9 m in depth and it is seen that the amplitude of the acceleration for $k=10^{-4}$ m/s possesses the value greater than that for $k=10^{-3}$ m/s.

Fig. 11 exhibits the effective stress paths in p-q plane at the depth 9.5 m. The liquefaction follows failure for $k=10^{-4}$ m/s in Fig. 11; however, the stress state for $k=10^{-3}$ m/s dose not reach liquefaction or failure. This result is similar to the ones obtained by Zienkiewicz et al.[23] and Oka et al.[21]. It is suggested that the occurrence of liquefaction is much dependent on the permeability coefficient of sand.

Fig. 12 demonstrates the relations between the effective mean principal stress p and depth. As seen in Fig. 12, p amounts to almost zero between 7 and 9.5 m in depth at 5.68 sec, i.e.,

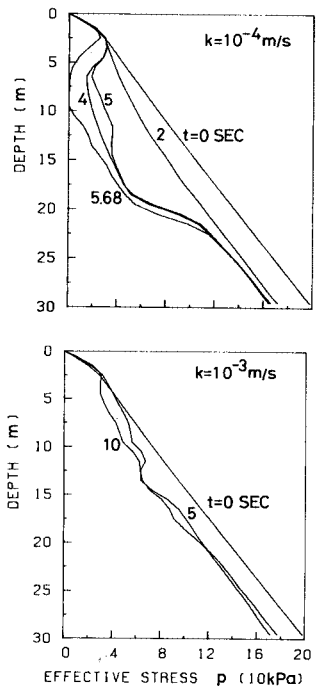

Fig. 12 Pore pressure profile.

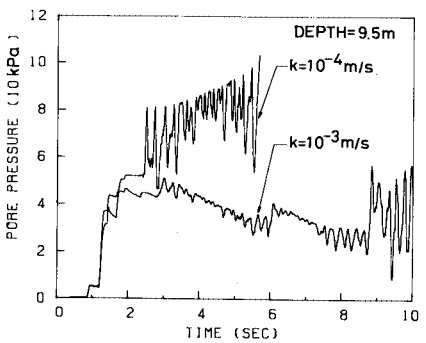

Fig. 13 Pore pressure time history.

liquefaction takes place. It may be of interest to note that the zone of liquefaction which Seed et al.[22] estimated on Niigata sand deposits is considerably similar to the depth range of liquefaction in Fig. 12. It is found, however, from Fig. 12 that the increase of the pore pressure for $k=10^{-3}$ m/s is not so conspicuous in comparison with $k=10^{-4}$ m/s.

Fig. 13 shows the relation between pore pressure and time at 9.5 m in depth. It is noticed that the pore pressure for $k=10^{-4}$ m/s increases with time, fluctuating after 2.5 sec to reach liquefaction, while for $k=10^{-3}$ m/s the increase of the pore pressure is not enough to cause liquefaction. Ishihara et al.[24] observed simultaneously the acceleration and the pore pressure in the sand deposits during an earthquake. The numerical result for $k=10^{-3}$ m/s in Fig. 13 is similar to the field data given by Ishihara et al. with respect to the trend that the pore pressure increases suddenly near the maximum value of the input acceleration and subsequently the dissipation of the pore pressure continues gradually.

Fig. 14 exhibits the effective vertical stress σ'_{22} at 9.5 m in depth. It is seen that σ'_{22} tends to decrease with time for $k=10^{-4}$ m/s; however, the trend for $k=10^{-3}$ m/s is that the effective stress σ'_{22} is increasing with not monotonous but fluctuating change on and after 2.5 sec. Fig. 15 shows the effective lateral stress σ'_{11} at the location 9.5 m in depth. The change of σ'_{11} for $k=10^{-4}$ m/s tends to decrease with fluctuating. When liquefaction occurs, the change of the total lateral stress σ_{11}, $\Delta\sigma_{11}$ can be written as $\Delta\sigma_{11}=(1-K_0)\sigma'_{22(0)}$, i.e., the total lateral stress increases as the state approaches liquefaction. This trend is also observed in experimental results shown by Ishihara et al.[25].

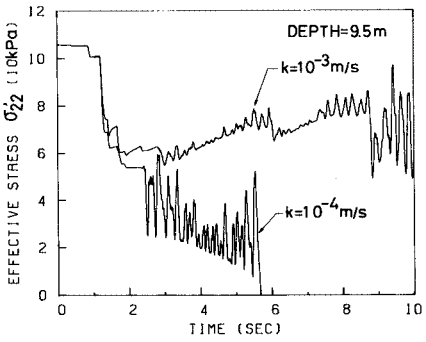

Fig. 14 σ'_{22} vs. time history.

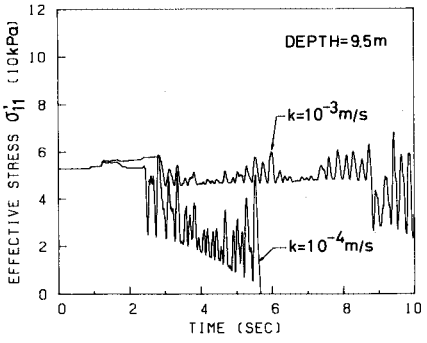

Fig. 15 σ'_{11} vs. time history.

5. CONCLUSIONS

The main results obtained in the present paper are summarized as follows:

(1) An elastic-plastic constitutive model of sand for cyclic loading is proposed by modifying the model available to monotonic loading conditions.

(2) A stress-strain relationship during repeated loads is derived from the non-associated flow rule violating Drucker's postulate.

(3) The incremental forms of the stress-strain relationship are presented to apply the constitutive model to the Finite Element method.

(4) The analytical formulation is made concerning the one-dimensional dynamic response of the level ground during an earthquake.

(5) For two cases where liquefaction occurs and does not appear, the characteristics of the effective stress path, liquefaction zone and pore pressure are demonstrated.

(6) The permeability coefficient makes significant influence on the response of the ground subjected to earthquakes.

REFERENCES

1) Jennings, P. C. : Periodic response of a general yielding structure, Proc. ASCE, No. EM 2, pp. 131~166, 1964.
2) Hardin, B. O. and Drnevich, V. P. : Shear modulus and damping in soils : design equations and curves, Proc. ASCE, No. SM 7, pp. 667~692, 1972.
3) Pande, G. N. and Zienkiewicz, O. C. : Soil mechanics-transient and cyclic loads, John Wiley & Sons, 1982.
4) Hirai, H., Yanagisawa, E. and Satake, M. : Elastic-plastic constitutive models for the behavior of sand, Proc. JSCE, No. 343, pp. 255~265, 1984.
5) Drucker, D. C. : A definition of stable inelastic material, J. Appl. Mech., Vol. 26, pp. 101~106, 1959.
6) Prager, W. : Recent developments in the mathematical theory of plasticity, J. Appl. Phys., Vol. 20, pp. 235~241, 1949.
7) Prevost, J. H. and Hoeg, K. : Soil mechanics and plasticity analysis of strain softening, Geotechnique, Vol. 25, No. 2, pp. 279~297, 1975.
8) Hill, R. : The mathematical theory of plasticity, Oxford Press, pp. 33~35, 1950.
9) Nova, R. : A constitutive model for soil under monotonic and cyclic loading, pp. 343~374, reference 3).
10) Mroz, Z. and Norris, V. A. : Elastoplastic and viscoplastic constitutive models for soils with application to cyclic loading, pp. 173~217, reference 3).
11) Dafalias, Y. F. and Herrmann, L. R. : Bounding surface formulation of soil plasticity, pp. 253~282, reference 3).
12) Nishi, K. : Elasto-plastic behaviour of saturated sand under undrained cyclic loading and its constitutive equation, Proc. JSCE, No. 319, pp. 115~128, 1982.
13) Ghaboussi, J. and Momen, H. : Modelling and analysis of cyclic behaviour of sands, pp. 313~342, reference 3).
14) Ishihara, K., Tatsuoka, F. and Yasuda, S. : Undrained deformation and liquefaction of sand under cyclic stresses, Soils and Foundations, Vol. 15, No. 1, pp. 29~44, 1975.
15) Drucker, D. C. and Prager, W. : Soil mechanics and plastic analysis or limit design, Quarterly Appl. Math., Vol. 10, pp. 157~165, 1952.
16) Biot, M. A. : Mechanics of deformation and acoustic propagation in porous media, J. Appl. Phys., Vol. 33, pp. 1482~1498, 1962.
17) Zienkiewicz, O. C. and Bettess, P. : Soils and other saturated media under transient, dynamic conditions ; general formulation and the validity of various simplifying assumptions, pp. 1~16, reference 3).
18) Zienkiewicz, O. C. : The finite element method in engineering science, McGraw-Hill, pp. 322~346, 1971.
19) Newmark, N. M. : A method of computation for structural dynamics, Proc. ASCE, Vol. 85, No. EM 3, pp. 67~94, 1959.
20) Zienkiewicz, O. C. and Parekh, C. J. : Transient field problems : two-dimensional and three-dimensional analysis by isoparametric finite elements, Int. J. Numerical Meth. Eng., Vol. 2, pp. 61~71, 1969.
21) Oka, F., Sekiguchi, K. and Goto, H. : A method of analysis of earthquake-induced liquefacthon of horizontally layered sand deposits, Soils and Foundations, Vol. 21, No. 3 pp. 1~17, 1981.
22) Seed, H. B. and Idriss, I. M. : Analysis of soil liquefaction : Niigata earthquake, Proc. ASCE, Vol. 93, No. SM 3, pp. 83~108, 1967.
23) Zienkiewicz, O. C., Leung, K. H., Hinton, E. and Chang, C. T. : Liquefaction and permanent deformation under dynamic conditions-numerical solution and constitutive relations, pp. 71~103, reference 3).
24) Ishihara, K., Shimizu, K. and Yamada, Y. : Pore water pressures measured in sand deposits during an earthquake, Soils and Foundations, Vol. 21, No. 4, pp. 85~100, 1981.
25) Ishihara, K. and Li, S. : Liquefaction of saturated sand in triaxial torsion shear stress, Soils and Foundations, Vol. 12, No. 2, pp. 19~39, 1972.

(Recieved May 30 1984)